Current Biology, Vol. 14, 1–10, January 6, 2004, ©2004 Elsevier Science Ltd. All rights reserved. DOI 10.1016/j.cub.2003.12.005

Dynamic Actin Patterns and Arp2/3 Assembly at the Substrate-Attached Surface of Motile Cells

Till Bretschneider,[1] Stefan Diez,[2] Kurt Anderson,[2] John Heuser,[3] Margaret Clarke,[4] Annette Müller-Taubenberger,[1] Jana Köhler,[1] and Günther Gerisch[1]*

[1]Max-Planck-Institut für Biochemie
D-82152 Martinsried
Germany

[2]Max-Planck-Institut für Molekulare Zellbiologie und Genetik
D-01307 Dresden
Germany

[3]Department of Cell Biology
Washington University School of Medicine
St. Louis, Missouri 63110

[4]Program in Molecular and Cell Biology
Oklahoma Medical Research Foundation
Oklahoma City, Oklahoma 73104

Summary

Background: In the cortical region of motile cells, the actin network rapidly reorganizes as required for movement in various directions and for cell-to-substrate adhesion. The analysis of actin network dynamics requires the combination of high-resolution imaging with a specific fluorescent probe that highlights the filamentous actin structures in live cells.

Results: Combining total internal reflection fluorescence (TIRF) microscopy with a method for labeling actin filaments, we analyze the dynamics of actin patterns in the highly motile cells of *Dictyostelium*. A rapidly restructured network of single or bundled actin filaments provides a scaffold for the assembly of differentiated actin complexes. Recruitment of the Arp2/3 complex characterizes stationary foci with a lifetime of 7–10 s and traveling waves. These structures are also formed in the absence of myosin-II. Arp2/3-actin assemblies similar to those driving the protrusion of a leading edge form freely at the inner face of the plasma membrane.

Conclusions: The actin system of highly motile cells runs far from equilibrium and generates a multitude of patterns within a dynamic filamentous network. Traveling waves are the most complicated patterns based on recruitment of the Arp2/3 complex. They are governed by the propagated induction of actin polymerization. We hypothesize that the actin system autonomously generates primordia of specialized structures such as phagocytic cups or lamellipodia. These primordia would represent an activated state of the actin system and enable cells to respond within seconds to local stimuli by chemotaxis or phagocytic-cup formation.

Introduction

The polymerization of actin at leading edges and the regulation of cell-to-substrate interactions are essential components of actin-based cell motility. Actin fulfils its functions within a cell by reversible polymerization into filaments. These filaments interact with myosin motor proteins and with a variety of regulatory proteins that force the filaments to form supramolecular complexes of different shapes. Other proteins anchor the filaments to membranes. In order to probe for the diversity of structures generated by the membrane-anchored actin-myosin system at the substrate-attached surface of living cells, we have applied total internal reflection fluorescence (TIRF) microscopy to the highly motile cells of *Dictyostelium*. TIRF microscopy selectively illuminates structures within an evanescent field extending only about 150 nm from the substrate surface into the cell. In *Dictyostelium* cells the membrane-anchored actin filament network has a thickness of 100–200 nm [1], meaning its entire structure is amenable to visualization by TIRF microscopy.

TIRF images are distinguished by a low contribution of background fluorescence from deeper layers in the cytoplasm, which is of particular importance for the imaging of protein complexes that exist in equilibrium with their diffusible subunits. TIRF microscopy has, for those reasons, become the method of choice for visualizing structures close to the substrate-attached surface of a cell [2–6]. To increase the sensitivity of TIRF microscopy for details of actin organization, it was necessary to combine this technique with the use of fluorescent probes that specifically interact with the filamentous form of actin. Here we present the first data on actin organization in live cells obtained by this advanced labeling and imaging procedure.

Dictyostelium cells resemble neutrophils in their capability to rapidly adjust their cortical actin system to environmental cues. Within seconds, both types of cells respond to adhering particles by forming a phagocytic cup and to chemoattractant by establishing a new leading edge [7].

Dictyostelium cells can project leading edges from any part of their surface, and their cortical actin system is re-organized within seconds to bring about changes in the direction of movement [8]. Quantitative TIRF analysis revealed a high turnover of spontaneously forming actin structures beneath the substrate-attached surface of these rapidly moving cells. Inserted into the network are dense actin tufts that are enriched in the Arp2/3 complex, one of the prominent regulators of the actin system [9]. In this paper we give an overview on the diversity and dynamics of actin-based patterns that are detected by TIRF microscopy at the substrate-attached surface of migrating *Dictyostelium* cells.

Results

Patterns of Actin, Arp2/3, and Myosin-II Assembly as Revealed by TIRF Microscopy

In order to study actin network organization at the substrate-attached surface of live cells of *Dictyostelium dis-*

*Correspondence: gerisch@biochem.mpg.de

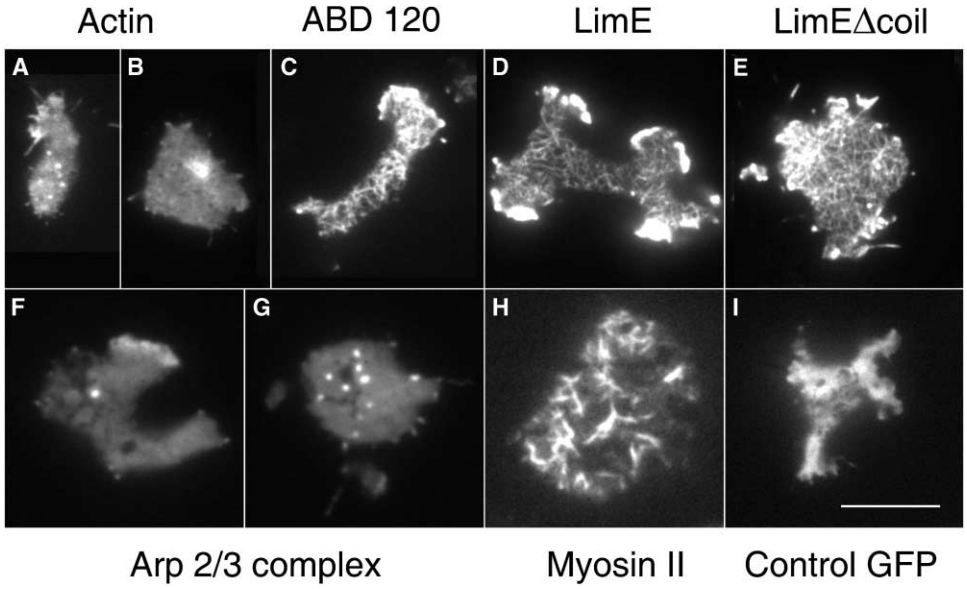

Figure 1. Patterns Formed by Actin, by the Arp2/3 Complex, and by Myosin-II at the Substrate-Attached Surface of *D. discoideum* Cells

(A and B) GFP-actin showing enrichment in cell surface extensions and in foci distributed over the cell-surface area.

(C)YFP-ABD120 visualizing a filamentous network into which strongly labeled foci are inserted.

(D) LimE-GFP expressed in LimE null cells, revealing network organization with high contrast against the low cytoplasmic background.

(E) LimEΔcoil-GFP expressed in myosin-II null cells.

(F and G) GFP-Arp3 recruited to a leading edge and assembled into discrete foci beneath the cell surface. Vesicles and tubules of the contractile vacuole system appear as dark structures against the GFP-Arp3 localized in the cytoplasm.

(H) GFP-myosin-II is organized into branched or interconnected filaments.

(I) Free GFP as a control. GFP or YFP fluorescence was recorded by TIRF microscopy in cells moving on a glass surface. The scale bar represents 10 μm.

coideum, we first applied TIRF microscopy to cells expressing GFP-actin, which is known to copolymerize with native actin [10]. Using GFP-actin as a fluorescent probe, we observed prominent accumulation at leading edges and in foci at the substrate-attached cell surface by TIRF microscopy (Figure 1A). However, only occasionally were network structures distinguishable from small diffuse clusters (Figure 1B). It appears that GFP-actin does not provide the contrast required for appropriate imaging of fine filament structures because it does not distinguish polymerized from nonpolymerized actin, which makes up about half of the total actin in a cell [11]. Therefore, to obtain sufficient contrast of actin network structures over cytoplasmic background, we combined TIRF microscopy with fluorescent probes that would preferentially label the filamentous actin.

We tagged two different types of probes with either green or yellow fluorescent protein (GFP or YFP) to visualize actin network dynamics. One consisted of the single actin binding domain of a filamin-like 120 kDa actin-crosslinking protein from *Dictyostelium* (ABD120). This probe was developed by Pang et al. [12] for the visualization of polymerized actin in living cells, and fitting the X-ray structure of a related domain, the domain 1 of fimbrin, to the helical structure of actin filaments clarified the structural basis of the probe's binding [13]. We derived a second probe from DdLimE, a LIM-domain containing protein that is strongly recruited to the actin cortex of *Dictyostelium* cells [14].

Both YFP-ABD120 and the LimE-GFP probes revealed a network of filaments beneath the substrate-attached surface of the cells (Figures 1C and 1D). Inserted into this network were brightly fluorescent structures of various shapes. At leading edges these structures formed a zone enriched in actin filaments, and at the substrate-attached cell surface they appeared as short-lived foci or propagating waves. The network architecture was seen equally sharply in mutant cells lacking myosin-II (Figure 1E), indicating that the action of conventional, double-headed myosin is not essential for the integrity of this dynamic actin network.

For most of the experiments, we have complemented LimE null cells with LimE-GFP in order to prevent endogenous LimE from competing with binding of the GFP-tagged LimE probe. The degree of LimE-GFP expression varied over a wide range, allowing us to determine that the patterns we observed are not artifacts caused by overexpression of the fusion protein. DdLimE contains at its C-terminal end a coiled-coil domain that is dispensable for binding to the actin cytoskeleton [15]. This domain has been eliminated in some of our constructs (LimEΔcoil) because the truncated protein revealed a particularly low cytoplasmic background. By parallel TIRF experiments, we established that the same type of actin patterns are formed when different LimE probes are used in the following combinations: LimEΔcoil tagged with GFP at either its N or C terminus in wild-type cells, full-length LimE tagged at its N or C terminus in wild-type cells, and full-length LimE-GFP or LimEΔcoil-GFP in LimE null cells.

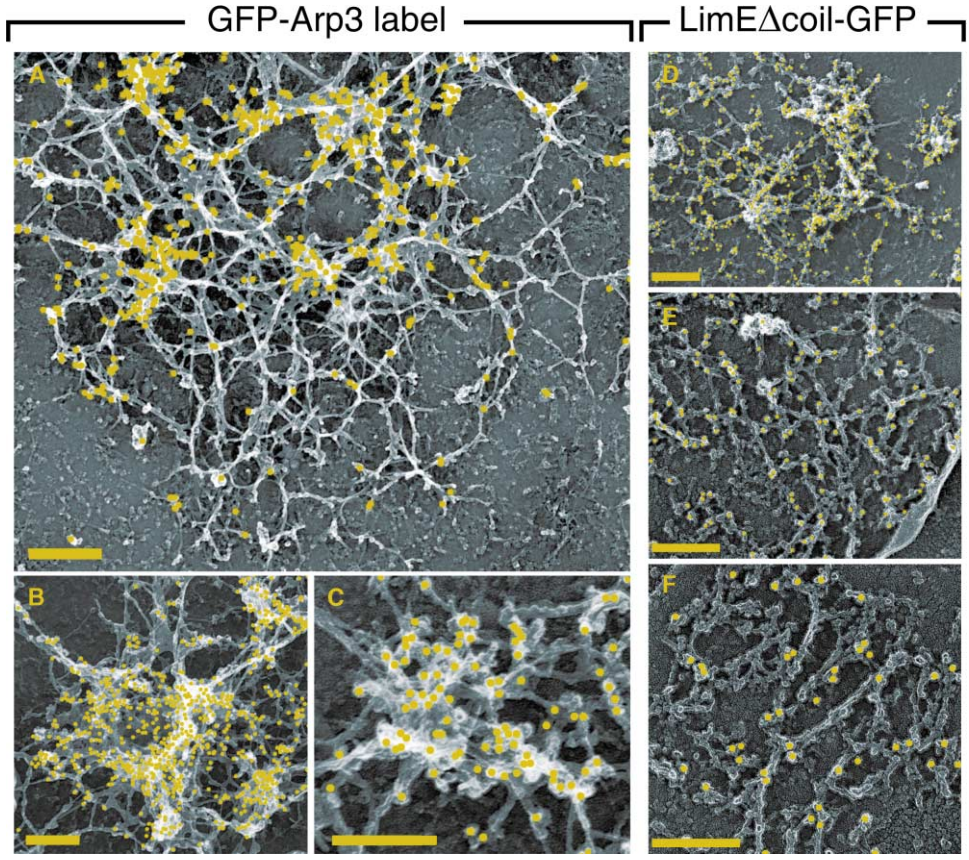

Figure 2. Electron Micrographs of Unroofed Cells of *D. discoideum*, Immunogold Labeled for the Localization of Arp2/3 or the LimEΔcoil Probe

Cells in the left panel expressed GFP-p41-Arc, which is marked by anti-GFP antibodies.

(A) Overview of actin organization at the bottom surface of a cell.

(B) A large cluster with extremely strong Arp2/3 labeling at sites of densest actin packing.

(C) Intersecting actin filaments in an Arp2/3-rich cluster.

Cells in the right panel expressed LimEΔcoil-GFP, which was immunogold labeled with anti-GFP antibodies.

(D) Overview.

(E and F) Images showing portions of the labeled actin network at higher magnifications. At the right side of (E), a fragment of the plasma membrane marking the cell border is seen. Antibody-conjugated gold particles are highlighted in yellow. Note that the loose network of actin filaments is labeled diffusely for LimE, whereas only the densest and most compact tufts of actin are labeled for the Arp2/3 complex. The scale bars represent 0.2 μm.

Two constituents of the Arp2/3 complex, Arp3 and p41-Arc, were enriched in foci similar to those formed by dense actin assemblies (shown for GFP-Arp3 in Figures 1F and 1G). The presence of myosin-II filaments at the substrate-attached cell surface was demonstrated by the use of myosin-II heavy chains tagged with GFP at their N-terminal head regions [16]. TIRF microscopy revealed the presence of interconnected myosin-II filaments that varied in thickness and shape (Figure 1H) and were in continuous reorganization (Movie 1 in the Supplemental Data available with this article online). The pattern of myosin-II assembly was distinct from the actin network structure; we have never observed GFP-myosin-II to build foci similar to those formed by Arp2/3-enriched actin assemblies.

Control cells with GFP alone showed only vesicular and tubular elements of the contractile vacuole system; these elements were recognizable in negative contrast as nonfluorescent areas against the uniform GFP fluorescence in the cytoplasm (Figure 1I).

To confirm that the structures visualized by the YFP-ABD120 and LimE-GFP probes are built from actin filaments, we treated cells with latrunculin A, a drug that sequesters G-actin into nonpolymerizable complexes [17, 18]. Within about 10 min, 5 μM latrunculin A caused release of the fluorescent probes into the cytoplasm in a uniformly dispersed state. Simultaneously, the entire cell became immobile and its membrane formed "pearling" extensions as described for transformed mouse fibroblasts [19]. After the latrunculin A was washed out, actin organization and cell motility completely recovered within half an hour (see Figure S2).

Immunogold Localization of Arp2/3 and LimE Probes

To correlate TIRF images with the ultrastructure of Arp2/3 assemblies and actin networks, we subjected cells expressing either GFP-tagged p41-Arc, a member of the Arp2/3 complex, or LimEΔcoil-GFP to electron

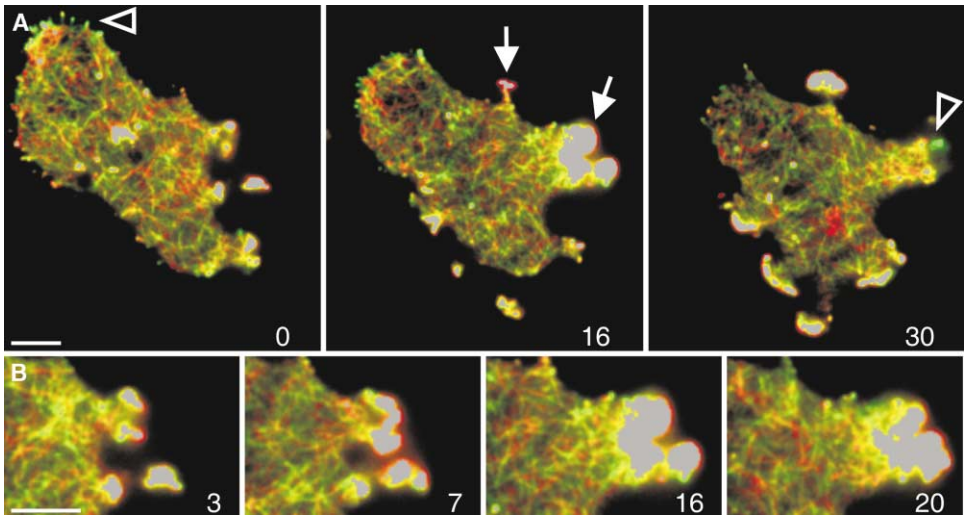

Figure 3. Dynamics of Actin Organization Visualized by LimEΔcoil-GFP in a LimE Null Background

TIRF images are taken from a time series recorded at 1 s intervals with exposure times of 100 ms for each image. For visualization of actin dynamics, two consecutive images are pseudocolored in green and red and superimposed on each other. Gray is used for regions having intensities that were above the upper threshold chosen for optimum display of the filament network.

(A) A cell in three stages of movement. Long filaments spanning half the length of the cell are evident in the right image. A new protrusion appears in the upper part of the middle image, and another one is expanding on the right (closed arrows). Retracting regions appear green (open arrowheads in the left and right images) and are accompanied by a dense texture of red, i.e., newly formed, filamentous elements at their base.

(B) A leading edge of the cell shown in (A) at four stages of protrusion. The red border of the edge represents the expansion within 1 s. Time is indicated in seconds after the first image of (A). Scale bars represent 5 μm.

microscopy. We "unroofed" the cells in order to expose the actin cytoskeleton associated with their substrate-attached membrane and then fixed and immunogold labeled the cells by using anti-GFP antibodies. The unroofed cells revealed at their bottom surface a network of mostly bundled actin filaments (Figure 2) comparable to the network structures visualized by TIRF microscopy (as shown in Figures 1C and 1D). In cells probed for the Arp2/3 complex, the actin filaments extended on the bottom surface of the cells were only rarely labeled (Figure 2A). The antibody labeling was especially concentrated on the dense actin clusters scattered within the network of filaments, in accord with the TIRF microscopic images shown in Figures 1F and 1G. Within the labeled clusters, the Arp2/3 complex was distributed throughout the entire volume from very close to the plasma membrane right up to the apices that penetrated most deeply into the cytoplasmic space (Figure 2B and Figure S1A). The actin filaments within these clusters did not show any preferential orientation (Figure 2C). Furthermore, there were no clathrin-coated structures associated with these foci of Arp2/3 enrichment.

LimEΔcoil-GFP as a marker gave an immunogold labeling pattern distinct from that of GFP-p41-Arc. As seen in overview (Figure 2D and Figure S1B), the labeled LimEΔcoil-GFP was distributed throughout the entire actin network. Vesicles associated with the substrate-attached surface of the cells were unlabeled, as was the cytoplasmic face of the plasma membrane beneath the actin network. High-power magnification revealed that the LimEΔcoil label was associated with most of the actin filaments and was not restricted to sites of filament branching or crosslinkage (Figures 2E and 2F).

Actin Network Dynamics at the Substrate-Attached Cell Surface

To visualize changes in actin network organization, we used TIRF microscopy to record cells expressing LimEΔcoil-GFP and superimposed consecutive frames from time series on each other. We pseudocolored the first frame in green and the second one in red. Network elements that disappeared from one frame to the other are thus seen in green, and elements that newly appeared are seen in red. Elements that remained at their position appear in a yellowish color. The images shown in Figure 3A indicate that within 1 s periods the filamentous network is continually restructured. Inserted into the network are foci of dense actin accumulation that are stationary relative to the substrate. Because linear contrast enhancement was applied to visualize actin filaments of low intensity, high-density structures such as foci or lamellipodia appear overexposed without any detailed substructure. Such regions have been colored gray in our images.

In Figure 3A, protruding and retracting regions of the cell are indicated by arrows and arrowheads, respectively. Protrusive activity occurs usually in a zone not more than 1 μm in width, wherein the packing density of actin filaments reaches a peak of about 5-fold the average density in the trailing loose network. Protrusion may also be linked to more discrete clusters of dense actin structures (Figure 3B). The loose actin network behind these clusters is being continually remodeled. Retracting areas are characterized by the abrupt appearance of new actin meshes at the base of the retracting region (Figure 3A and Movie 2). These meshes may act

as transient supports for myosin-II filaments, which generate the force needed for retraction [16].

Quantification of Actin Dynamics in Ventral Foci

The foci transiently formed at the substrate-attached cell surface proved to be best suited for quantitative studies on actin assembly and Arp2/3 recruitment (Movie 3). For both GFP-tagged actin and Arp3, the temporal changes in fluorescence intensity were characterized by sharp peaks with a full width of 7 to 10 s at half-maximal fluorescence intensity (Figures 4A–4C). These dynamics imply that the polymerization of actin is abruptly followed by depolymerization and that the accumulation of Arp2/3 complexes is followed by their dispersal. The temporal profiles of both actin and Arp2/3 were slightly asymmetric. The increasing branches could be well fitted by exponential curves, and they were shorter than the decreasing branches, which had a less-defined shape. For GFP-Arp3, similar data were collected from cells immobilized by compression with an agar sheet, establishing that the program of Arp2/3 recruitment to each focus of assembly is independent of leading-edge activities and global movement of the cell (Figure 4D). Data obtained with GFP-p41-Arc, another constituent of the Arp2/3 complex, confirmed that the dynamics of GFP-Arp3 are representative of the entire complex (data not shown).

To evaluate any influence that myosin-II may have on focal assembly and disassembly, we expressed GFP-actin in myosin-II null mutants. As shown in Figure 4E, the rates of assembly and disassembly in myosin-II null cells were close to those in wild-type cells (Figure 4B).

Because LimEΔcoil-GFP associates with filamentous actin in a noncovalent manner, the velocity of binding will depend on its association rate. For an estimate of whether binding of the probe faithfully reports the polymerization and depolymerization of actin within the cells, we have compared foci visualized by the indirect LimEΔcoil-GFP label with foci into which GFP-actin was directly incorporated. The overall shape of the curves was similar (Figure 4F as compared to 4B). For actin, the average half-time of the increasing branch was $T1/2\uparrow = 2.03$ (± 0.29) s, and that of the decreasing branch was $T1/2\downarrow = 3.65$ (± 0.38) s (numbers in parentheses are 99% confidence limits of the means). For LimEΔcoil-GFP, the corresponding numbers were $T1/2\uparrow = 1.69$ (± 0.27) and $T1/2\downarrow = 3.64$ (± 0.45) s. In conclusion, no significant differences were observed in a comparison of half-times of the increasing and decreasing branches obtained by the direct or indirect labeling of actin.

There are two possibilities for how foci may arise and disappear; actin filaments may shuttle into the focus and back into its vicinity, or actin may be polymerized de novo and depolymerized in situ. Although we would not rule out an exchange of actin filaments, the data shown in Figures 4G and 4H argue for a major contribution of local polymerization and depolymerization. If actin filaments are attracted from a larger distance, they should be gradually condensed into a sharp focus; if they are recruited from the immediate vicinity, a zone surrounding a focus should be depleted of polymerized actin. No evidence for either event is provided by the profiles shown in Figures 4G and 4H.

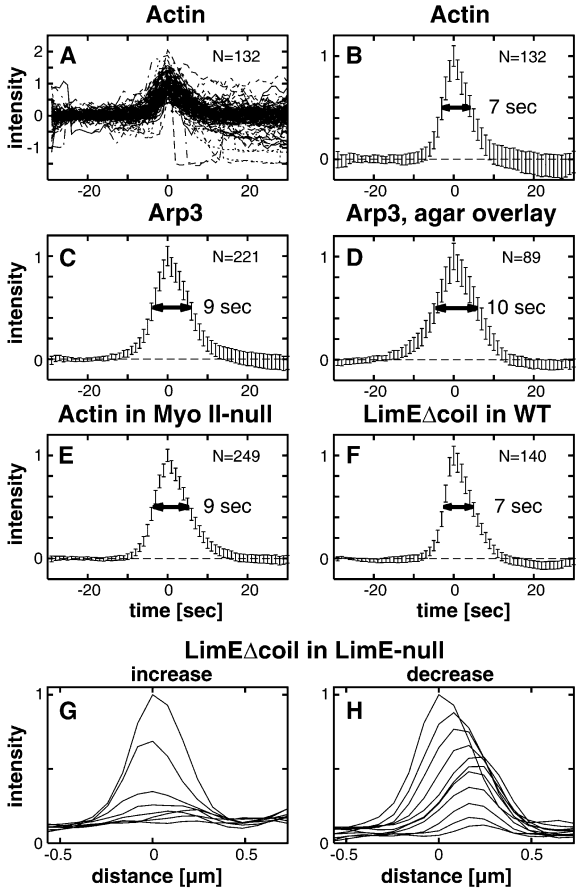

Figure 4. Temporal Profiles of Actin and Arp2/3 Assembly and Disassembly in Foci at the Substrate-Attached Cell Surface

Increases and decreases of fluorescence intensity were recorded by TIRF microscopy, and the data from N measurements were aligned according to their peak values.

(A) Original data for GFP-actin illustrating narrow deviations from average in spite of larger variations in a few runs.

(B) Calculated average for GFP-actin incorporation in wild-type cells.

(C) Fluorescence intensities of GFP-Arp3 in cells freely moving on a glass surface (as in [A] and [B]).

(D) GFP-Arp3 in cells compressed by agar overlay.

(E) GFP-actin as in (B), but in myosin-II null cells.

(F) Fluorescence intensities in foci labeled with LimEΔcoil-GFP in a wild-type background.

(G and H) Spatial profiles of fluorescence intensity in line scans through a focus. Curves are plotted at 0.5 s intervals during formation (G) and at 1.0 s intervals during decay (H) of a focus. Double arrows in (B) to (F) indicate full width at half maximum of the peaks. The vertical bars demarcate 99% confidence limits of the mean. For fitting of the curves see the Experimental Procedures.

Arp2/3-Based Waves of Actin Polymerization

The most complicated spatio-temporal patterns generated at the substrate-attached cell surface are traveling waves of dense actin assembly. A cell generating multiple wave patterns of actin assembly is displayed in Figure 5A, with the contrast adjusted to visualize the low-intensity network of actin filaments. Development of the

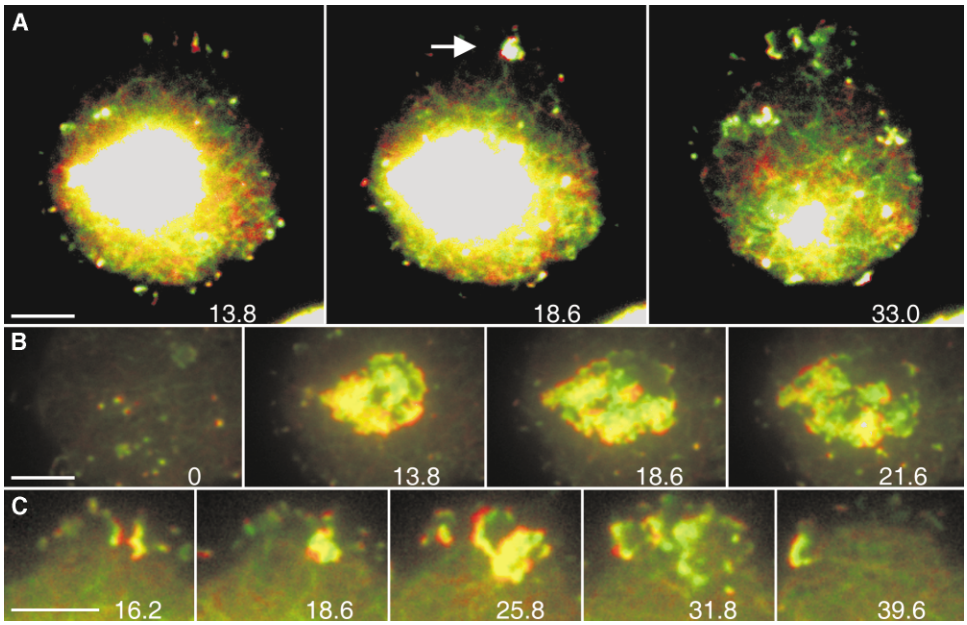

Figure 5. Wave Patterns of Dense Actin Assembly

(A) Cell showing multiple waves embedded into a network of actin filaments visualized by LimE-GFP in a LimE null background. The cell is shown at three stages, with contrast enhanced in order to visualize the filamentous network.

(B) Middle region of this cell shown at the same magnification but with contrast appropriate to distinguish structures within the central area. The four stages illustrate pattern development immediately before emergence of the first wave (0 s), during propagation of the first wave front (at 13.8 s), at the emergence of a second wave (red kernel at 18.6 s), and during propagation of this wave (red front and green center at 21.6 s).

(C) Traveling waves from the upper region of the cell (white arrow in [A]). Red and green coloring of images taken at 1.2 s intervals is the same as in Figure 3. The cell has been slightly compressed by agar overlay. Time is indicated in seconds after the first frame in (B). For comparison of the sequences of (A), (B), and (C), the 18.6 s frame is shown as a reference in each series. The scale bars represent 5 μm.

wave pattern in the middle of this cell is displayed with contrast optimized for this region in Figure 5B and supplementary Movie 4. A special case of wave initiation is documented in Figure 5C; the waves in the upper region of the cell (arrow in Figure 5A) emerged from the collision of two dense actin assemblies. These waves traveled at an average velocity of 15 $\mu m \times min^{-1}$ until they became finally integrated into the border of the cell (Figure 5C and Movie 5).

We addressed the question of whether the propagated waves of actin assembly are linked to folds of the plasma membrane by combining the GFP-LimE-Δcoil marker for waves with a red fluorescent membrane label. The styryl dye FM4-64 integrates instantaneously into the plasma membrane and subsequently labels endosomes and the contractile vacuole system of *Dictyostelium* cells [20]. Figure 6 shows a time series of two cells recorded by dual-emission TIRF microscopy. The cell in the upper part of each frame forms two actin waves on its substrate-attached cell surface (Figure 6D, arrows in the 70 s frame). Increased fluorescence intensity of the membrane label is evident where the fronts of the two cells overlap (Figure 6E, arrow at 0 s), indicating that an overlay of membranes is detectable in these images. No such increase in membrane fluorescence accompanied the spreading of waves, indicating that actin waves can travel on an essentially planar membrane (Figure 6F).

The propagation of actin waves may reflect translocation of polymerized Arp2/3-actin clusters, which may be moved by the action of a motor protein or by the force of actin polymerization (Figures 7A and 7B), similar to particles propelled by a comet tail of actin [21, 22]. Alternatively, wave propagation may be an autocatalytic process based on the induction of actin polymerization at the wave front and actin depolymerization at the back of the wave (Figure 7C). To distinguish between these alternatives, we have searched for wave patterns displaying discrete clusters that can be monitored for changes in position. Stationary clusters together with the appearance of new ones at the front of a wave would indicate an induction process. The analysis of Arp2/3 patterns provided evidence that the waves indeed propagate by sequential induction. The clusters of Arp2/3 assemblies remained stationary when the waves passed beyond them, and the rear boundary of the waves was defined by the disassembly of these structures (Figures 7D and 7E; Movie 6).

Discussion

Dynamics of Actin Network Organization

Dictyostelium cells are representative of rapidly moving cells capable of adapting their activities to various environmental influences and of rapidly changing their shape in response to external signals. In particular, neu-

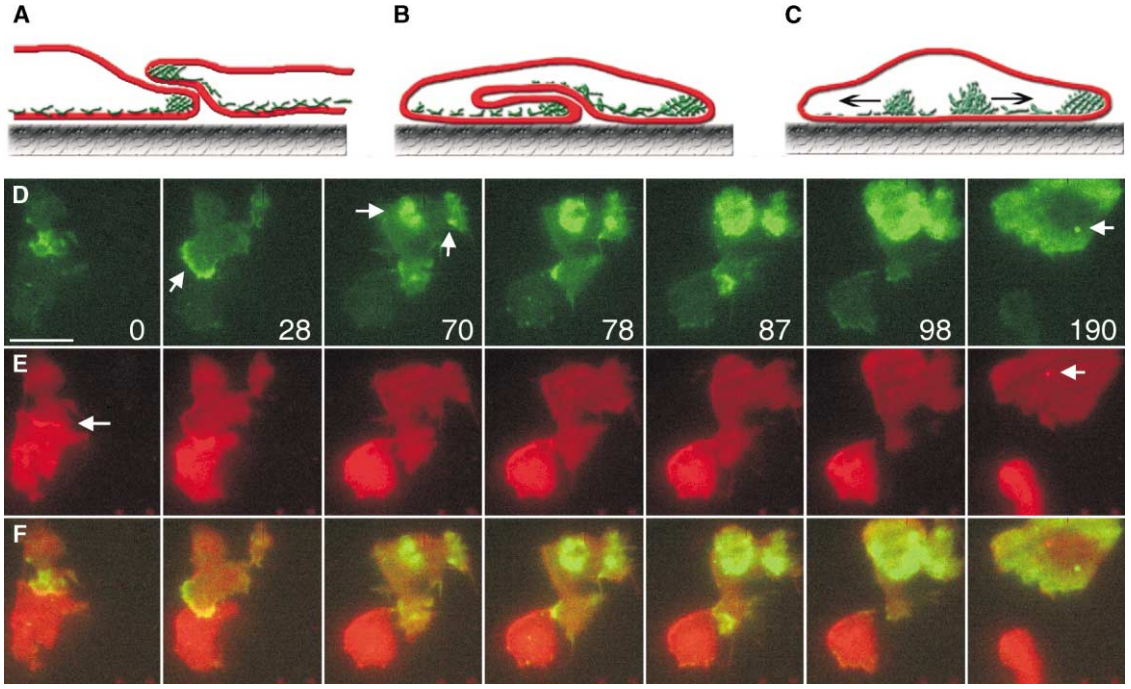

Figure 6. TIRF Images of Actin Wave Patterns in Combination with a Membrane Label to Demonstrate Independence of Wave Propagation from Membrane Folding

(A–C) Schematic sections through cells moving on a solid surface illustrate potential actin-membrane relationships in traveling waves. The plasma membrane is drawn in red, and actin-filament structures close to the substrate surface are in green. (A) Two partially overlapping cells. (B) One cell with undercutting lamellipod. The similarity of membrane arrangements suggests that case (B) should be detectable by TIRF microscopy if case (A) is detectable. In (C), actin waves are proposed to travel on the inner face of an essentially planar membrane. (D and E) In cells expressing GFP-LimEΔcoil in a wild-type background, membranes were labeled with FM4-64, a red fluorescent dye added at 11 min before the recording started. Time is indicated in seconds after the first frame. (D) GFP fluorescence visualizing traveling waves of actin assembly. (E) FM4-64 fluorescence of membranes. (F) Superimposition of the LimEΔcoil and membrane labels. In (D), three types of structures are indicated by arrows: a leading edge (28 s frame), traveling waves (70- to 98 s frames), and the focal assembly of actin (190 s frame). In (E), overlay of the membranes of two cells is indicated by an arrow in the zero frame. In the 190 s frame an intracellular vesicle is indicated, most likely an endosome moving along a microtubule as described previously [32]. This spot shows that additional membrane area, even of a small size, is easily detected. The scale bar represents 10 μm.

trophils resemble *Dictyostelium* cells in their phagocytic and chemotactic activities, as well as in their fast migration within heterogeneous environments. The cells of *Dictyostelium* generate specialized actin-based structures at any site of their surface. Leading edges or endocytic cups are formed either spontaneously or within seconds upon local stimulation.

In this report we focus on the pattern and dynamics of actin-filament assembly far away from, and independent of, a leading edge. Of central interest is the mechanism governing the propagation of actin waves along the inner surface of a substrate-attached cell membrane (Figures 5 and 6). The actin network associated with the bottom surface of a *Dictyostelium* cell consists of crosslinked single and bundled actin filaments (Figure 2). The faintest filamentous structures we can resolve by TIRF within a living cell appear to be tiny actin bundles. A rough estimate is obtained by the use of filopods, which contain bundles of 6-16 actin filaments in cross-section (Ohad Medalia, personal communication based on cryo-electron tomographic data), as a reference. The average fluorescence intensity in network elements was about one-third of that in filopods and corresponded to 2–5 filaments per bundle.

TIRF microscopy as used here in combination with appropriate probes for the labeling of actin filaments can be exploited for various cell types in order to examine alterations in the dynamics and structure of actin networks. For instance, changes that are caused by deficiencies in myosin motors or in regulatory proteins that control actin polymerization, membrane-association, or the crosslinkage of actin filaments can be visualized by this technique. Further studies are needed to clarify whether the observed changes reflect actin polymerization or myosin-based gliding movement of preexisting filaments, or perhaps a blend of both activities.

TIRF microscopy also proved to be the method of choice for visualizing filament dynamics of myosin-II. The extended network of myosin-II filaments at the substrate-attached cell surface provides an excellent opportunity to study the dynamics of these filaments in vivo. Myosin-II is known to be concentrated primarily at the rear of a moving cell, where it is responsible for retraction of the tail [16]. Close to the substrate surface, myosin-II filaments may function in promoting detachment of the cells. Myosin-II null cells are more flattened than wild-type cells and less effective in detaching from sticky substrates [23].

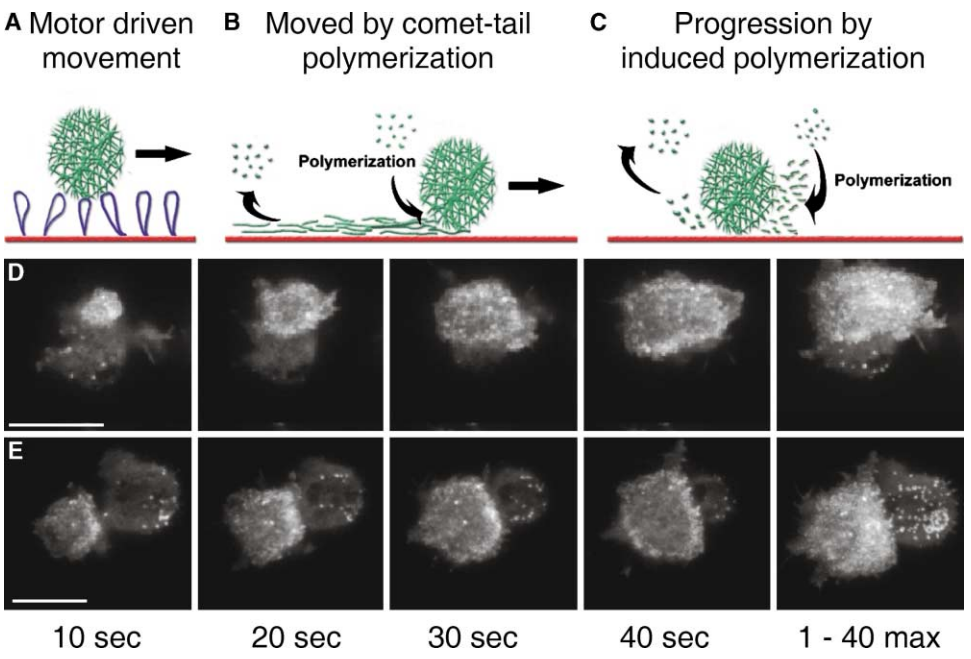

Figure 7. Propagated Induction of Arp2/3 Assembly as a Basis for Traveling-Wave Formation

(A–C) To illustrate three potential mechanisms of actin wave propagation, cross-sections through a wave are diagrammed as dense actin clusters (green) that travel on the inner face of the plasma membrane (red). (A) Movement of the cluster by a myosin motor protein (blue). (B) Movement of the cluster by actin polymerization at its back, the actin filaments forming a tail behind the cluster. (C) Propagated induction of actin polymerization in front of the cluster is accompanied by actin dissociation at its back. In this case, wave propagation does not reflect the transport of a persisting actin assembly. (D and E) TIRF images of two cells at 10 s intervals show discrete clusters of GFP-Arp3 within traveling waves. Outside of the waves, typical foci of transient Arp2/3 assembly are visible. Maximum projections shown in the right panels represent the maximum intensity attained by a pixel in images acquired every second within the total period of 40 s. These projections demonstrate that clusters that form part of the traveling waves are essentially stationary relative to the substrate. Moving clusters would be traced in the form of stripes. Scale bars represent 10 μm.

Foci and Traveling Waves

Embedded within the dynamic network and sharing the Arp2/3 complex as a major constituent are short-lived foci and traveling waves of high actin filament density. In the foci, a rapid local increase in polymerized actin is followed by a sharp fall (Figure 4), suggesting an intrinsic program of actin assembly and disassembly. The arrangement of actin filaments in these foci is consistent with a high degree of branching caused by the Arp2/3 complex (Figure 2). Actin filaments appear to be branched in the clusters or crosslinked at various angles, and they are often bundled, in line with cryo-electron tomographic data on other regions of the cell cortex [24]. The texture of foci is consistent with the presence of other proteins in addition to constituents of the Arp2/3 complex [8, 25, 26]. The foci in *Dictyostelium* cells belong to a family of Arp2/3-enriched actin spots observed in various cell types. Such spots are formed throughout the lamella of PtK1 fibroblasts [21]. These spots are motile, located to the upper cell surface, and associated with fin-like projections of the cell membrane. Unlike podosomes in macrophages [27], the foci of *Dictyostelium* cells are not primed close to the leading edge but are initiated throughout the substrate-attached cell surface (Movie 3). Most importantly, these Arp2/3-enriched dense actin assemblies are not associated with clathrin-coated pits or vesicles (Figure 2 and Figure S1A). They are distinguished, therefore, from the actin plumes transiently formed when clathrin-coated structures move from the plasma membrane into the cytosol [3]. Immobility of the foci could be due to their association with cell adhesion proteins that are attached to the substrate surface in the plasma membrane.

The Arp2/3-actin waves studied in this paper are dynamic patterns that are generated in the cell cortex by the polymerization of actin and recruitment of associated proteins [8, 28]. These waves may be related to arc-like arrays of eupodia, actin-rich structures that *Dictyostelium* cells protrude into a soft substrate such as an agar surface [29]. The waves we observed are structures spreading in two dimensions above a solid, plane glass surface. Because of this geometry, the traveling waves provide a model system amenable to TIRF microscopy for self-organization of actin-filament assembly in single cells. It will be a crucial question to address whether activators of the Arp2/3 complex, such as WASp or WAVE, which normally link actin polymerization to the protrusion of a leading edge, will also guide a wave of actin polymerization when it is uncoupled from membrane protrusion.

Conclusions

The combination of TIRF microscopy with specific probes for actin network structures and sites of Arp2/3 recruitment revealed a high potential of dynamic pattern formation at rapidly moving cells' substrate-attached

surface, apart from the membrane of a leading edge. Short-lived foci are of interest from a practical point of view. Their well-defined assembly and disassembly kinetics render them appropriate for the assays of drug effects on actin dynamics. The most complicated patterns formed, traveling waves of Arp2/3-actin coassembly, are based on a self-sustained induction process; these waves are propagated by the coordinated de-novo assembly of actin in association with the Arp2/3 complex. In this respect, the traveling-wave phenomenon resembles the continued actin polymerization at a leading edge. There is, however, a major difference. At leading edges, actin polymerization is proposed to be nucleated by membrane-associated activators of the Arp2/3 complex, primarily WASp and N-WASP, which determine the direction of polymerization and link it to membrane protrusion [9]. In traveling waves, actin is not polymerizing against a membrane barrier at the front of these waves, which instead appear to reflect autonomous pattern formation in the actin system (Figure 6). In conclusion, the actin network provides a dynamic matrix in the cell cortex and allows regulatory proteins such as the Arp2/3 complex to generate a variety of specialized structures at the substrate-attached cell surface.

A functional implication of the fast turnover of actin structures detected in this study is the plasticity of the cell cortex. This enables cells to undergo fast shape changes in accord with the requirements of life in a heterogeneous environment and to respond rapidly to local stimuli. We propose that the actin system spontaneously generates foci of Arp2/3 accumulation outside of a leading edge and thus explores the environment in a search for signals. Chemoattractants or adhering particles may stabilize and amplify these primordia of specialized actin structures and convert them into a leading edge or a phagocytic cup.

Experimental Procedures

TIRF Microscopy of Live Cells and Image Processing

Cells of the *D. discoideum* strain AX2-214 were used for expression of fluorescent fusion proteins. The myosin-II null strain HS1 expressing GFP-myosin-II heavy chains [16] was kindly provided by J. A. Spudich. Cells were cultivated in nutrient medium in polystyrene culture dishes at 23°C and were washed twice in 17 mM K/Na - phosphate buffer (pH 6.0) before TIRF imaging. Where indicated, the cells were compressed by agar overlay [30].

Through-the-objective TIRF microscopy was performed with standard coverslips and conventional immersion oil. For Figures 3 and 5, red/green colored consecutive frames were superimposed with ImageJ software (http://rsb.info.nih.gov/ij/) with customized macros and plugins. For superimposition, individual 16 bit frames were background subtracted before fixed contrast enhancement was applied to all frames of a time series. After conversion to 8 bit, the sequence was duplicated and pseudocolored. The first frame of the red and the last frame of the green channel were deleted. Each composite RGB image contains an original frame at time t in green merged with an original frame at time $t + \Delta t$ in red. Merging the channels into a 24 bit RGB stack resulted in images as shown in Figures 3 and 5. Gray is used to characterize pixel values that are above the upper threshold set in the contrast enhancement procedure. For example, the original data used for Figure 3A contain pixel values between 0 and 11784 out of the 65535 values obtainable with the 16 bit CCD camera. In order to highlight the low-intensity actin network structures, we chose a pixel value of 2393 as the upper threshold.

Electron Microscopy and Immunogold Labeling

Cells were unroofed by an ultrasonic burst as described by Heuser [31]. After fixation in 2% formaldehyde, the unroofed cells were incubated with affinity-purified rabbit anti-GFP antibodies and subsequently labeled with goat anti-rabbit antibodies conjugated to 12 nm gold. After freeze-drying, the specimen was subjected to rotary replication with platinum.

Supplemental Data

Vector construction for GFP-LimE fusion proteins and YFP-ABD120 and details of the TIRF and electron-microscopic techniques are described in the Supplemental Data available with this article online at http://www.current-biology.com/cgi/content.full/14/1/1/DC1/.

Acknowledgments

We thank Emmanuel Burghardt and Ursula Mintert for their collaboration, Josipa Bilic for construction of the YFP vector, and Evelyn Simmeth for figure graphics. This work was supported by grants from the Deutsche Forschungsgemeinschaft (GE 135/20 to G.G.), the US Public Health Service (National Institutes of Health grant GM29647 to J.E.H.), the National Science Foundation (MCB-9728403 to M.C.), and the Oklahoma Center for the Advancement of Science and Technology (HR01-024 to M.C.) and by a fellowship of the Schloessmann Foundation to T.B.

Received: October 13, 2003
Revised: November 7, 2003
Accepted: November 10, 2003
Published: January 6, 2004

References

1. Hanakam, F., Albrecht, R., Eckerskorn, C., Matzner, M., and Gerisch, G. (1996). Myristoylated and non-myristoylated forms of the pH sensor protein hisactophilin II: Intracellular shuttling to plasma membrane and nucleus monitored in real time by a fusion with green fluorescent protein. EMBO J. *15*, 2935–2943.
2. Krylyshkina, O., Anderson, K.I., Kaverina, I., Upmann, I., Manstein, D.J., Small, J.V., and Toomre, D.K. (2003). Nanometer targeting of microtubules to focal adhesions. J. Cell Biol. *161*, 853–859.
3. Merrifield, C.J., Feldman, M.E., Wan, L., and Almers, W. (2002). Imaging actin and dynamin recruitment during invagination of single clathrin-coated pits. Nat. Cell Biol. *4*, 691–698.
4. Neuhaus, E.M., Almers, W., and Soldati, T. (2002). Morphology and dynamics of the endocytic pathway in *Dictyostelium discoideum*. Mol. Biol. Cell *13*, 1390–1407.
5. Steyer, J.A., and Almers, W. (2001). A real-time view of life within 100 nm of the plasma membrane. Nat. Rev. Mol. Cell Biol. *2*, 268–275.
6. Axelrod, D. (1989). Total internal-reflection fluorescence microscopy. Methods Cell Biol. *30*, 245–270.
7. Devreotes, P.N., and Zigmond, S.H. (1988). Chemotaxis in eukaryotic cells - A focus on leukocytes and *Dictyostelium*. Annu. Rev. Cell Biol. *4*, 649–686.
8. Bretschneider, T., Jonkman, J., Köhler, J., Medalia, O., Barisic, K., Weber, I., Stelzer, E.H.K., Baumeister, W., and Gerisch, G. (2002). Dynamic organization of the actin system in the motile cells of *Dictyostelium*. J. Muscle Res. Cell Motil. *23*, 639–649.
9. Pollard T.D., Borisy G.G. (2003). Cellular motility driven by assembly and disassembly of actin filaments. Cell *112*, 453–465 (113, 549 Erratum).
10. Westphal, M., Jungbluth, A., Heidecker, M., Mühlbauer, B., Heizer, C., Schwartz, J.M., Marriott, G., and Gerisch, G. (1997). Microfilament dynamics during cell movement and chemotaxis monitored using a GFP-actin fusion protein. Curr. Biol. *7*, 176–183.
11. Haugwitz, M., Noegel, A.A., Karakesisoglou, J., and Schleicher, M. (1994). Dictyostelium amoebae that lack G-actin-sequestering profilins show defects in F-actin content, cytokinesis, and development. Cell *79*, 303–314.
12. Pang, K.M., Lee, E., and Knecht, D.A. (1998). Use of a fusion

protein between GFP and an actin-binding domain to visualize transient filamentous-actin structures. Curr. Biol. *8*, 405–408.
13. Hanein D., Volkmann N., Goldsmith S., Michon A.M., Lehman W., Craig R., DeRosier D., Almo S., and Matsudaira P. (1998). An atomic model of fimbrin binding to F-actin and its implications for filament crosslinking and regulation. Nat. Struct. Biol. *5*, 787–792 (*5*, 924 Errata).
14. Prassler, J., Murr, A., Stocker, S., Faix, J., Murphy, J., and Marriott, G. (1998). DdLIM is a cytoskeleton-associated protein involved in the protrusion of lamellipodia in *Dictyostelium*. Mol. Biol. Cell *9*, 545–559.
15. Schneider, N., Weber, I., Faix, J., Prassler, J., Müller-Taubenberger, A., Köhler, J., Burghardt, E., Gerisch, G., and Marriott, G. (2003). A Lim protein involved in the progression of cytokinesis and regulation of the mitotic spindle. Cell Motil. Cytoskeleton *56*, 130–139.
16. Moores, S.L., Sabry, J.H., and Spudich, J.A. (1996). Myosin dynamics in live *Dictyostelium* cells. Proc. Natl. Acad. Sci. USA *93*, 443–446.
17. Pring, M., Cassimeris, L., and Zigmond, S.H. (2002). An unexplained sequestration of latrunculin A is required in neutrophils for inhibition of actin polymerization. Cell Motil. Cytoskeleton *52*, 122–130.
18. Spector, I., Shochet, N.R., Blasberger, D., and Kashman, Y. (1989). Latrunculins - novel marine macrolides that disrupt microfilament organization and affect cell-growth.1. Comparison with Cytochalasin-D. Cell Motil. Cytoskeleton *13*, 127–144.
19. Bar-Ziv, R., Tlusty, T., Moses, E., Safran, S.A., and Bershadsky, A. (1999). Pearling in cells: A clue to understanding cell shape. Proc. Natl. Acad. Sci. USA *96*, 10140–10145.
20. Heuser, J., Zhu, Q.L., and Clarke, M. (1993). Proton pumps populate the contractile vacuoles of *Dictyostelium* amoebae. J. Cell Biol. *121*, 1311–1327.
21. Schafer, D.A., Welch, M.D., Machesky, L.M., Bridgman, P.C., Meyer, S.M., and Cooper, J.A. (1998). Visualization and molecular analysis of actin assembly in living cells. J. Cell Biol. *143*, 1919–1930.
22. Thompson, C., Lin, C.H., and Forscher, P. (1996). An Aplysia cell adhesion molecule associated with site-directed actin filament assembly in neuronal growth cones. J. Cell Sci. *109*, 2843–2854.
23. Jay, P.Y., Pham, P.A., Wong, S.A., and Elson, E.L. (1995). A mechanical function of myosin-II in cell motility. J. Cell Sci. *108*, 387–393.
24. Medalia, O., Weber, I., Frangakis, A.S., Nicastro, D., Gerisch, G., and Baumeister, W. (2002). Macromolecular architecture in eukaryotic cells visualized by cryoelectron tomography. Science *298*, 1209–1213.
25. Robinson, D.N., Ocon, S.S., Rock, R.S., and Spudich, J.A. (2002). Dynacortin is a novel actin bundling protein that localizes to dynamic actin structures. J. Biol. Chem. *277*, 9088–9095.
26. Insall, R., Müller-Taubenberger, A., Machesky, L., Köhler, J., Simmeth, E., Atkinson, S.J., Weber, I., and Gerisch, G. (2001). Dynamics of the *Dictyostelium* Arp2/3 complex in endocytosis, cytokinesis, and chemotaxis. Cell Motil. Cytoskeleton *50*, 115–128.
27. Evans, J.G., Correia, I., Krasavina, O., Watson, N., and Matsudaira, P. (2003). Macrophage podosomes assemble at the leading lamella by growth and fragmentation. J. Cell Biol. *161*, 697–705.
28. Vicker, M.G. (2002). F-actin assembly in *Dictyostelium* cell locomotion and shape oscillations propagates as a self-organized reaction-diffusion wave. FEBS Lett. *510*, 5–9.
29. Fukui, Y., and Inoue, S. (1997). Amoeboid movement anchored by eupodia, new actin-rich knobby feet in *Dictyostelium*. Cell Motil. Cytoskeleton *36*, 339–354.
30. Fukui, Y., Yumura, S., and Yumura, T.K. (1987). Agar-overlay immunofluorescence - High-resolution studies of cytoskeletal components and their changes during chemotaxis. Methods Cell Biol. *28*, 347–356.
31. Heuser, J. (2000). The production of 'cell cortices' for light and electron microscopy. Traffic *1*, 545–552.
32. Clarke, M., Köhler, J., Heuser, J., and Gerisch, G. (2002). Endosome fusion and microtubule-based dynamics in the early endocytic pathway of *Dictyostelium*. Traffic *3*, 791–800.